Clinical Biomechanics 100 (2022) 105827

Contents lists available at ScienceDirect

Clinical Biomechanics

journal homepage: www.elsevier.com/locate/clinbiomech

Prediction of cerebral perfusion pressure during carotid surgery – A computational fluid dynamics approach

Madelene Holmgren [a,*], Petter Holmlund [a], Karen-Helene Støverud [a,b], Laleh Zarrinkoob [c,d], Anders Wåhlin [a,e,f], Jan Malm [c], Anders Eklund [a,f]

[a] Department of Radiation Sciences, Radiation Physics, Biomedical Engineering, SE 901 87 Umeå University, Umeå, Sweden.
[b] Department of Health Research, SINTEF Digital, NO 7465 Trondheim, Norway
[c] Department of Clinical Science, Neurosciences, Umeå University, SE 901 87 Umeå, Sweden
[d] Department of Surgical and Perioperative Sciences, Umeå University, SE 901 87 Umeå, Sweden
[e] Department of Applied Physics and Electronics, Umeå University, SE 901 87 Umeå, Sweden
[f] Umeå Center for Functional Brain Imaging, Umeå University, SE 901 87 Umeå, Sweden

ARTICLE INFO

Keywords:
Endarterectomy
Carotid stenosis
Computational fluid dynamics
Ischemic stroke
Magnetic resonance imaging

ABSTRACT

Background: Maintaining cerebral perfusion pressure in the brain when a carotid artery is closed during vascular surgery is critical for avoiding intraoperative hypoperfusion and risk of ischemic stroke. Here we propose and evaluate a method based on computational fluid dynamics for predicting patient-specific cerebral perfusion pressures at carotid clamping during carotid endarterectomy.

Methods: The study consisted of 22 patients with symptomatic carotid stenosis who underwent carotid endarterectomy (73 ± 5 years, 59–80 years, 17 men). The geometry of the circle of Willis was obtained preoperatively from computed tomography angiography and corresponding flow rates from four-dimensional flow magnetic resonance imaging. The patients were also classified as having a present or absent ipsilateral posterior communicating artery based on computed tomography angiography. The predicted mean stump pressures from computational fluid dynamics were compared with intraoperatively measured stump pressures from carotid endarterectomy.

Findings: On group level, there was no difference between the predicted and measured stump pressures (−0.5 ± 13 mmHg, $P = 0.86$) and the pressures were correlated ($r = 0.44$, $P = 0.039$). Omitting two outliers, the correlation increased to $r = 0.78$ ($P < 0.001$) (−1.4 ± 8.0 mmHg, $P = 0.45$). Patients with a present ipsilateral posterior communicating artery ($n = 8$) had a higher measured stump pressure than those with an absent artery ($n = 12$) ($P < 0.001$).

Interpretation: The stump pressure agreement indicates that the computational fluid dynamics approach was promising in predicting cerebral perfusion pressures during carotid clamping, which may prove useful in the preoperative planning of vascular interventions.

1. Introduction

The cerebral perfusion pressure is driving the cerebral blood flow. For cerebral protection, a maintained perfusion pressure becomes critical during vascular interventions when the blood flow through a major supplying artery is closed, such as in carotid endarterectomy (CEA) (Howell, 2007). During CEA, the atherosclerotic plaque is removed while the blood flow through the carotid artery is temporality closed by clamping the artery (Howell, 2007). Monitoring of the cerebral perfusion during CEA aims to identify patients at risk for perioperative complications and need for shunting, in which carotid blood flow can be reestablished (Wiske et al., 2018). Currently there is no consensus about which single monitoring technique that best distinguishes patients who would need shunting (Naylor et al., 2018; Wiske et al., 2018), but clinically used monitoring methods during general anesthesia include electroencephalography, somatosensory evoked potentials, near-infrared spectroscopy, transcranial doppler, and stump pressure (Domenick Sridharan et al., 2018; Hans and Jareunpoon, 2007; Jonsson et al., 2017; Moritz et al., 2007). In addition, the individual configuration and collateral function of the cerebral circulation might be

* Corresponding author at: Department of Radiation Sciences, Umeå University, 901 87 Umeå, Sweden.
E-mail address: madelene.holmgren@umu.se (M. Holmgren).

https://doi.org/10.1016/j.clinbiomech.2022.105827
Received 20 May 2022; Accepted 18 November 2022
Available online 19 November 2022

overlooked in preoperative planning (AbuRahma et al., 2011; Merkkola et al., 2006; Müller et al., 2021; Pennekamp et al., 2013). The common purpose of these approaches is to identify signs of low perfusion on the clamped side, motivating development of a quantitative method for establishing the individual prerequisites for sufficient cerebral perfusion when clamping a carotid artery.

The stump pressure is measured distal to the clamped artery and is the resulting pressure from a collateral compensation via the major cerebral arteries forming the circle of Willis, intended to reflect the perfusion pressure in the distal vasculature, such as the ipsilateral middle and anterior cerebral artery territories (Fig. 1). We have recently applied computational fluid dynamics (CFD) in a cohort of patients with symptomatic carotid stenosis, for simulating the patient-specific blood pressure distribution in the circle of Willis (Holmgren et al., 2021). These patients underwent CEA, and in this paper, we further developed our CFD-model for simulating the intraoperative state when clamping the carotid artery.

Using intraoperatively measured mean stump pressures as a reference, we aimed to validate the CFD model based on angiographic and flow velocity imaging before surgery, for predicting cerebral intra-arterial pressures in the circle of Willis at carotid clamping during CEA. A secondary aim was to investigate how the anatomical variations of the circle of Willis contributed to the resulting pressure distribution.

2. Methods

Patients with symptomatic carotid stenosis that underwent CEA were preoperatively investigated with computed tomography angiography (CTA) and four-dimensional phase-contrast magnetic resonance imaging (4D flow MRI). A CFD model with a two-step approach was developed for patient-specific simulations of the arterial pressure distributions. The model was based on a segmented arterial tree from CTA for well-defined geometries, blood flow from 4D flow MRI as the required inflow and outflow to the model, and mean arterial pressure (MAP) as pressure input to the calculations. The circle of Willis geometry consisted of an anterior part including the left and right internal carotid arteries (ICA), proximal middle cerebral arteries (MCA1), proximal and distal anterior cerebral arteries (ACA1, ACA2) and the anterior communicating arteries (ACoA), and a posterior part including the basilar artery (BA), the proximal and distal posterior cerebral arteries (PCA1, PCA2) and the posterior communicating arteries (PCoA) (Fig. 1).

2.1. Patients

The study population consisted of 22 patients (73 ± 5 years, range 59–80 years, 17 men) with ischemic stroke or transient ischemic attack and who underwent CEA. The patients had symptomatic carotid stenosis ≥50%, with or without non-symptomatic contralateral stenosis. Inclusion criteria were modified Rankin Scale score < 3 and Mini-Mental State Exam >23 (Folstein et al., 1975; van Sweiten et al., 1988). Full details about inclusion and exclusion criteria are presented in the original recruitment (Zarrinkoob et al., 2019). Patient characteristics are presented in Table 1. The study population was part of a previous modeling study (Holmgren et al., 2021), from which we excluded six patients because they had no CEA surgery ($n = 3$) or unavailable stump pressures (n = 3).

Blood pressures from two occasions were used in the analysis. 1) The blood pressure was regularly taken non-invasively at the stroke ward, and the last blood pressure taken at rest the day before CEA was recorded. 2) The blood pressure during CEA was continuously monitored using an arterial line in the radial artery. The MAP at clamping and the mean stump pressure were obtained from the surgical records. In one patient, the MAP was missing, and the median value of the group was instead used for this patient.

During general anesthesia, phenylephrine was used as the vasopressor for increasing the blood pressure. Sevoflurane with minimum alveolar concentration 0.5 together with infusion remifentanil was used for general anesthesia. The systolic blood pressure was increased aiming for 150 mmHg before clamping, according to the surgical protocol. The common and external carotid arteries were clamped, and the stump

Table 1
Characteristics of patients.

***N* = 22**	
Age (mean, range)	73 ± 5 (59–80)
Sex (F/M)	5/17
Systolic blood pressure before surgery (mmHg)	138 ± 19
Diastolic blood pressure before surgery (mmHg)	70 ± 10
Mean arterial pressure before surgery (mmHg)	93 ± 11
Mean arterial pressure during clamping (mmHg)	101 ± 7
Heart rate (bpm)	65 ± 12
MMSE	27 ± 2
mRS (median, range)	0 (0–1)
NIHSS (median, range)	1 (0–6)
Symptomatic stenosis (%)	75 ± 12
Contralateral stenosis (%)	37 ± 28*
Diabetes mellitus (n)	5
Hyperlipidemia (n)	13
Hypertension (n)	17
Ever smoker (n)	13

Mean ± SD (range), *All 22 patients.
MMSE, Mini-Mental State Exam; mRS, modified Ranking Scale; NIHSS, National institutes of Health Stroke Scale.

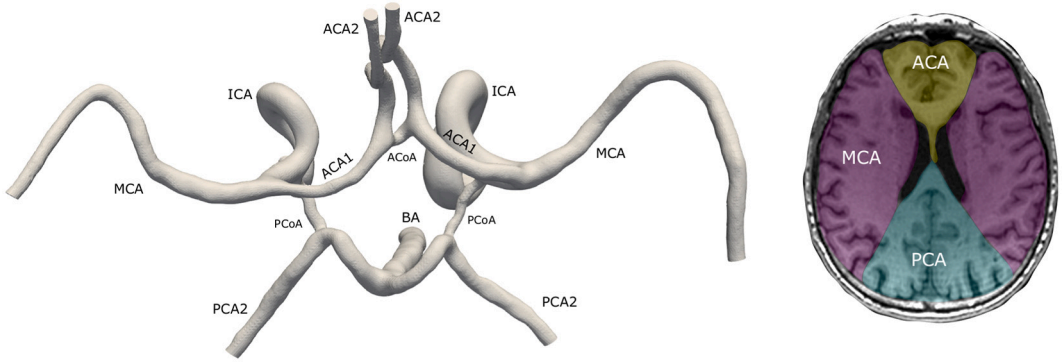

Fig. 1. Circle of Willis and vascular territories. The major cerebral arteries connecting to the circle of Willis are depicted to the left, where branches from these arteries have been removed. To the right is a schematic representation of the three major vascular territories. Supplying arteries are the internal carotid arteries (ICA) and the basilar artery (BA). The ICAs supply the anterior circulation consisting of the anterior cerebral artery (ACA) and the middle cerebral artery (MCA) territory. The BA supplies the posterior circulation consisting of the posterior cerebral artery (PCA) territory. The posterior communicating arteries (PCoA) connect the anterior and posterior circulation. The anterior communicating artery (ACoA) connects the right and left sides of the anterior circulation, i.e., the left and right ACA.

pressure was measured distal to the clamping as a single measurement. The target stump pressure limit for shunt insertion was a mean arterial stump pressure < 50 mmHg.

The study was approved by the ethical review board at Umeå University (Dnr: 2011–440-31 M) and the Swedish Ethical Review Authority (Dnr: 2019–05909). It was performed in accordance with the guidelines of the Declaration of Helsinki. Oral and written information about the study was given to all participants, and written consent was obtained from all participants.

2.2. Classification of patients

Patients were classified as having a present ipsilateral PCoA ($n = 8$) if it was visible in the CTA images, an absent PCoA ($n = 12$) if it was not visible, or fetal ($n = 2$) if the PCA1 segment was missing and PCoA was the sole supplier of the PCA2 (Table 2). Patients with both ipsi- and contralateral stenoses with a degree of stenosis ≥50% ($n = 9$) were classified as having bilateral stenoses (Table 2). Patients defined as a unilateral stenosis had a degree of stenosis of ≥50% only on the ipsilateral side. Each stenosis was graded according to the method in the North american symptomatic carotid endarterectomy trial (1991).

2.3. 4D flow MRI for blood flow rate assessment

4D flow MRI was performed before surgery using a 3 T scanner (GE Discovery MR 750, Milwaukee, WI, USA) with a 32-channel head coil. Scans with full brain coverage were performed in approximately nine minutes, using the PC-VIPR sequence (vastly undersampled isotropic projection reconstruction) (Gu et al., 2005; Johnson and Markl, 2010). Velocity-encoding was 110 cm/s and isotropic voxel size 0.68 × 0.68 × 0.68 mm^3. Details for the MRI settings have previously been described (Holmgren et al., 2021). Velocity data were post-processed for flow rate quantification to obtain mean flow rates (Holmgren et al., 2020). Mean blood flow rates were measured in the left and right MCA1, ACA1, ACA2, PCA2, and the ipsilateral PCoA. The positive PCoA flow direction was defined from ICA to PCA2. Because the high-venc 4D flow MRI is less sensitive for detecting low or absent flow, and no contrast agent was used, these images were not optimized for anatomical vessel segmentation.

2.4. CTA for segmentation of the arterial tree

Patient-specific geometries of the circle of Willis were segmented from clinical CTA images scanned at each patient's local hospital, with reconstructed slice thickness ranging between 0.3 and 0.625 mm, and trans-axial image resolutions ranging between 0.33 and 0.625 mm. Segmentations were performed with Synopsys' Simpleware™ software (ScanIP P-2019.09; Synopsys, Inc., Mountain View, USA). The CTA images were cropped to only include the circle of Willis, and interpolated to obtain isotropic voxels of 0.3 or 0.3125 mm. An edge-preserving bilateral filter was used for reducing background noise from surrounding tissue. The vessel walls were detected by an initial image intensity threshold, followed by the gradient-based filter 'Local surface correction'. A volume and topology preserving smoothing filter was applied prior to model generation.

Table 2
Overview of patients and presence of the ipsilateral PCoA and a contralateral stenosis.

	n	Unilateral	Bilateral
All	22	13	9
Present PCoA	8	5	3
Absent PCoA	12	7	5
Fetal PCoA	2	1	1

PCoA, ipsilateral posterior communicating artery.

2.5. CFD modeling

The arterial geometries were meshed for CFD and generated with the Simpleware FE module and imported as meshes into COMSOL Multiphysics® (COMSOL Multiphysics®, version 5.4, www.comsol.com, COMSOL AB, Stockholm, Sweden). The meshes were generated with a target edge length equal to the interpolated voxel size, and four boundary layers. See Holmgren et al. (2021) for more details regarding the mesh.

For obtaining the pressure distributions in the arteries, Navier-Stokes equations were solved with the CFD-module in COMSOL Multiphysics. The flow was assumed laminar, and the blood was assumed to be an incompressible Newtonian fluid with density ρ=1060 kg/m^3 and viscosity μ=3.45 mPa·s. The vessel walls were assumed rigid and impermeable. A no-slip condition was applied to the vessel walls.

2.6. Cerebral pressure prediction

Stationary CFD simulations for the intraoperative pressure predictions were performed in two steps. First, the cerebrovascular territorial resistances were determined from a simulation with fully developed laminar flow rates at the inlet (ICA and BA) and outlet (MCA, ACA and PCA2) boundaries (Fig. 2a), corresponding to the preoperative state. These flow rates were acquired from 4D flow MRI. We used the MAP measured preoperatively and applied it as a pressure point constraint at the contralateral ICA. For patients with bilateral stenoses, the inlet pressure at the contralateral ICA was set to MAP minus the pressure drop over the stenosis (see section 2.7). The main simulation output was the arterial pressures at each outlet (P_{out}).

In this first simulation step, we always omitted the contralateral PCoA ($n = 4$) for securing the correct flow rate in the ipsilateral PCoA. Because no outlet or inlet boundary was applied at the PCoAs, this was a way of maintaining the flow distribution between the two PCA1 segments corresponding to the 4D flow MRI measurements. These contralateral PCoAs were included in the second simulation.

Each distal territorial resistance (R_{out}) was found by dividing the cerebral perfusion pressure, i.e., the difference between the P_{out} and the intracranial pressure (ICP), by the measured flow in each distal artery (Q)

$$R_{out} = \frac{P_{out} - ICP}{Q}$$

The ICP was assumed to be 11.6 mmHg for all patients (Holmgren et al., 2020; Malm et al., 2011).

In the second simulation step, the boundary conditions were altered to imitate the intraoperative state. Artery-specific variable pressure boundary conditions were defined at each outlet of the circle of Willis (Fig. 2b). Each pressure was calculated by integration of the simulated velocity $\boldsymbol{u}$ across the outlet boundary $\boldsymbol{S}$ in the normal direction $\boldsymbol{n}$, multiplied by the distal flow resistance, yielding

$$P = R_{out} \int (\boldsymbol{u} \bullet \boldsymbol{n})\, dS + ICP$$

The R_{out} and ICP were assumed constant. The R_{out} was assumed to be the same before and during surgery, i.e., no autoregulatory response was included in the analysis. Importantly, no flow rates had to be specified with this implementation, meaning that the 4D flow MRI data is not used in the second simulation step, since these boundary conditions now allowed the flow rates to self-adjust according to the inlet pressure condition and the outflow resistances. The intraoperatively measured MAP at clamping was applied at the contralateral ICA and BA inlet, implemented as a fully developed laminar flow with a pressure condition. In patients with bilateral stenoses, the contralateral ICA inlet was replaced by a variable pressure condition with a flow resistance acquired from the separate stenosis simulation (see section 2.7), and by using MAP as the baseline pressure instead of the ICP. We applied a no-slip

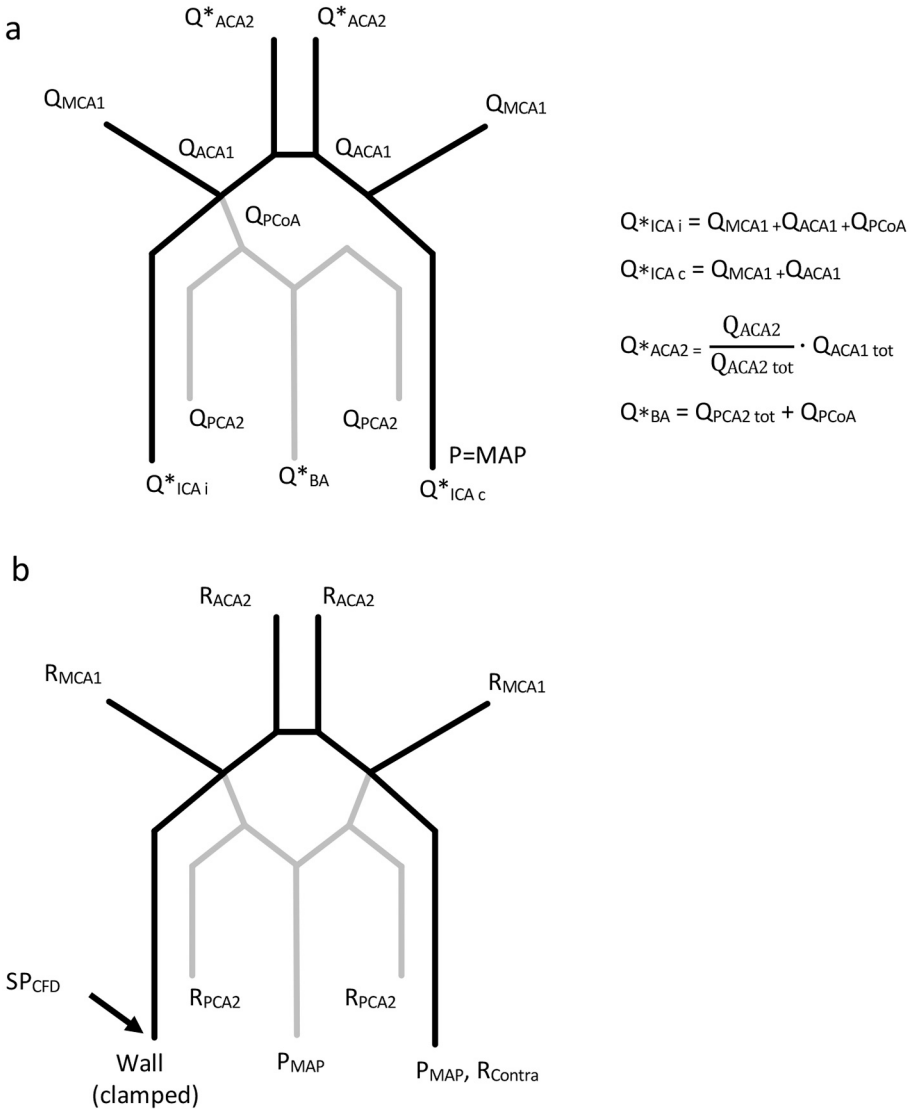

$$Q^*_{ICA\ i} = Q_{MCA1} + Q_{ACA1} + Q_{PCoA}$$

$$Q^*_{ICA\ c} = Q_{MCA1} + Q_{ACA1}$$

$$Q^*_{ACA2} = \frac{Q_{ACA2}}{Q_{ACA2\ tot}} \cdot Q_{ACA1\ tot}$$

$$Q^*_{BA} = Q_{PCA2\ tot} + Q_{PCoA}$$

Fig. 2. Schematic drawing of CFD boundary conditions. **a)** Flow rate boundary conditions (Q) for simulations used to obtain outlet vascular resistances. The anterior circulation is in black, and the posterior is in gray. The posterior part was only included in a subset of the patients where the ipsilateral PCoA was visible. The contralateral PCoA was always omitted for securing correct flow rates in the ipsilateral PCoA, but were included in the second simulation step. Flow rates denoted with * were calculated from measured 4D flow MRI flow rates according to the requirement of mass conservation. The ICA inlets are denoted ipsilateral (i) and contralateral (c) relative to the side with the ICA stenosis. **b)** Boundary conditions for simulations used to predict stump pressures, where resistances (R) are used as constants in the variable pressure boundary condition. The left side of the figure is the ipsilateral side with the stump pressure measured at the previous ICA inlet, now applied as a no-slip condition, i.e., wall. For patients with a contralateral stenosis, P_{MAP} was changed to a variable pressure condition with resistances from separate stenosis simulations.

condition at the ipsilateral ICA inlet boundary, corresponding to a clamped ICA with no flow. As initial values, we added the MAP to the whole geometry. For improvement of simulation stability, the blood viscosity was ramped in two distinct steps, by ten and one times the viscosity. The solution for the higher viscosity was used as the initial solution to the second step. The stump pressure was estimated as the average pressure at the ipsilateral ICA boundary.

The average pressure at the ipsilateral ICA boundary wall was compared with the measured stump pressure.

2.7. Contralateral stenosis simulation

In patients with bilateral carotid stenoses, we segmented the contralateral stenoses and performed CFD simulations for obtaining the correct MAP at the intracranial ICA inlet, and for avoiding assumptions about the contralateral ICA blood flow rates. Based on the simulations, we computed each stenosis flow resistance. The segmentations covered the carotid bifurcation, including parts of the common carotid artery (CCA) and the external carotid artery (ECA) (Fig. S1). The segmentations were performed in the same way as for the circle of Willis but with substantial manual corrections in the cases with narrow stenoses. The boundary conditions for these simulations were: 4D flow MRI-assessed outflow at the ICA (C3-C4 level), 100 mL/min outflow in ECA based on values from the literature (Marshall et al., 2004; Zarrinkoob et al., 2015). The sum of these two flow rates was used at the inlet in the common carotid artery. A zero-pressure reference point was also placed at the inlet. The resistance was calculated from the flow through the ICA and the resulting pressure drop across the stenosis. These simulations were dynamic, and the flow rate was ramped up during 0.1 s from a low-flow stationary solution (approximately 10 mL/min) to improve convergence. Convergence for the simulated pressure drop was acquired after less than one simulated second.

2.8. Effects on stump pressure

The effects of a contralateral stenosis on the stump pressure were assessed by performing simulations without compensating for the contralateral stenosis resistance and pressure drop.

Since controlling MAP is a way to maintain perfusion pressure during surgery, we wanted to investigate how increases in MAP were transferred to the stump pressure. It was investigated by repeating the stump pressure simulations with an increased MAP of 10 mmHg at the contralateral ICA and BA inlets.

Blood flow rates in ICA, BA, and MCA were investigated by comparing the mean blood flow rates from the preoperative MRI investigation and the CFD-simulated flow rates during clamping. The

CFD mean flow rates were found by integrating the velocities at the inlet and outlet boundaries.

2.9. Statistical analysis

All mean values were presented as the mean ± standard deviation. The main analysis was performed on the whole study population, where the predicted stump pressures from the CFD model (SP_{CFD}) were compared to stump pressures measured at clamping (SP_{Meas}). Two-tailed paired *t*-tests were used to test significance between predicted and measured stump pressures. Subgroup analysis investigated functional causes of reduced stump pressures, and was performed with respect to the contralateral stenosis and the presence of the ipsilateral PCoA. Correlations were assessed with Pearson's linear correlation coefficient. Tukey's fences were used to identify outliers in the data, i.e., data points lying beyond quartiles 1 and 3 by a distance of 1.5 times the interquartile range (or more). The significant level was set as $P < 0.05$.

3. Results

In the 22 patients, the SP_{Meas} during surgery was 57 ± 13 mmHg. Five of the 22 patients received a shunt (their stump pressure range being 40–53 mmHg).

The SP_{CFD} versus the SP_{Meas} is shown in Fig. 3. The SP_{CFD} was 56 ± 12 mmHg. There was no difference between the pressures (−0.5 ± 13 mmHg, $P = 0.86$) (Table 3) and a significant correlation of $r = 0.44$ ($P = 0.039$). Omitting two outliers (for potential explanation, see discussion), the correlation was $r = 0.78$ ($P < 0.001$) and the difference − 1.4 ± 8.0 mmHg ($P = 0.45$). An illustration of the pressure distribution in a typical subject is shown in Fig. 4.

Omitting the effects of the contralateral stenosis in the bilateral stenosis group led to an increase in the SP_{CFD} by 14 ± 13 mmHg ($P = 0.01$, $n = 9$).

When simulating an increase in MAP by 10 mmHg, we found a general SP_{CFD} increase of 4.2 ± 1.3 mmHg for the entire group ($P < 0.001$). The SP_{CFD} elevation was 5.0 ± 0.7 mmHg ($n = 8$) for subjects with a present ipsilateral PCoA, and 3.6 ± 1.3 mmHg ($n = 12$) for subjects with an absent ipsilateral PCoA ($P < 0.02$ when comparing the two groups).

Comparing the measured stump pressures revealed an average of 18 mmHg higher mean pressure in the patients with a present ipsilateral PCoA compared to patients with an absent ipsilateral PCoA ($P < 0.001$) (Table 3).

When comparing MRI-measured preoperative flow rates with CFD-simulated flow rates during clamping we observed that the ipsilateral MCA flow rate was significantly decreased in patients with an absent ipsilateral PCoA, and for patients with unilateral stenoses (Table 3). A comparison of flow rates in the ICA, BA, and MCA is provided in Supplementary Table S1.

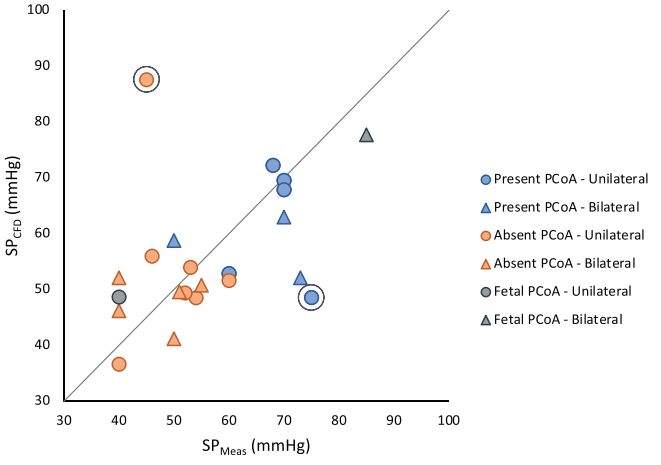

Fig. 3. Predicted stump pressure (SP_{CFD}) versus measured stump pressure (SP_{Meas}). Subgroups indicate those with a present ipsilateral posterior communicating artery (PCoA), absent PCoA, and two cases with fetal PCoA. Cases marked with triangles are patients with bilateral stenoses. According to Tukey's fences criteria, two patients (circled) could be regarded as outliers. Full line marks line of equality.

Table 3
Comparison of measured (SP_{Meas}) and simulated (SP_{CFD}) stump pressures. In addition, comparison of blood flow rates in the middle cerebral artery (MCA), between measured preoperative flow rates from 4D flow MRI and CFD-simulated flow rates during clamping of the carotid artery (OP).

		Stump pressure (mmHg)			Blood flow rate (ml/min)		
	n	SP_{Meas}	SP_{CFD}	P	MCA Pre	MCA OP	P
All	22	57 ± 13	56 ± 12	0.86	123 ± 24	91 ± 39	<0.001*
Present PCoA	8	67 ± 8	61 ± 9	0.18	128 ± 25	117 ± 43	0.29
Absent PCoA	12	49 ± 7	52 ± 12	0.46	115 ± 23	69 ± 14	<0.001*
Fetal PCoA[a]	2	63	63		144	121	
Unilateral stenosis	13	56 ± 12	57 ± 13	0.85	126 ± 27	90 ± 38	0.001*
Bilateral stenosis	9	57 ± 16	55 ± 11	0.40	118 ± 21	93 ± 41	0.07

SP, stump pressure; PCoA, ipsilateral posterior communicating artery.
[a] No statistical analysis, *P < 0.05.

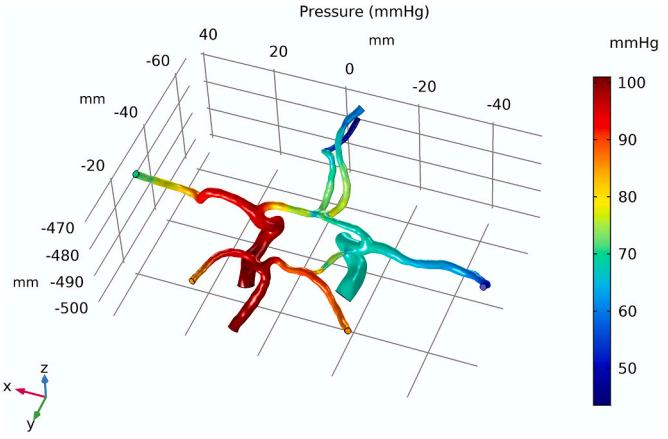

Fig. 4. Pressure distribution from a computational fluid dynamic simulation of one patient with a present ipsilateral posterior communicating artery, seen from the upper posterior view. The ipsilateral side is to the right in the image. The predicted stump pressure for this patient was 68 mmHg, and the measured stump pressure was 70 mmHg. Mean arterial pressures at the inlets were 100 mmHg.

4. Discussion

We proposed and evaluated a CFD approach to predict the pressure distribution in the circle of Willis during clamping of a carotid artery. No group difference was found between the predicted and measured stump pressures, and the methods were well correlated. The simulations indicate that the CFD approach was promising in predicting intraoperatively measured perfusion pressures, which may prove useful in the preoperative planning of surgical interventions.

4.1. Patient-specific model approach

A major strength of our CFD model approach was using 4D flow MRI, which provided simultaneous blood flow rates in all cerebral arteries for use as boundary conditions in the CFD model (Dunås et al., 2019; Wåhlin et al., 2021).This allowed us to simulate individual pressure distributions within the cerebral arteries (Holmgren et al., 2021), providing estimations of all vascular territorial resistances. Similar to our study, Berg et al. (2014) used flow rates as both inlet and outlet boundary conditions in a CFD model to investigate velocity fields in the circle of Willis. They only analyzed three individuals but highlighted the importance of precise MR data as boundary conditions.

Using the territorial-specific resistances, we took this method a step further by predicting the patient-specific perfusion pressures during carotid clamping, with validations against in-vivo pressure measurements. The pressure in the middle cerebral artery in case of an occluded or clamped carotid artery has been investigated with lumped models of the circle of Willis (Cassot et al., 2000; Cieslicki and Ciesla, 2005; Matsuura et al., 2021). The models have been based on literature data, limiting generalizability on an individual basis. Although a couple of studies have investigated the pressure distribution in the circle of Willis in case of a stenosis in the carotid artery (Liu et al., 2017; Schollenberger et al., 2021), the number of cases were few and not translated to the change in hemodynamics in the clamped case. In short, using 4D flow MRI in combination with CFD is a novel approach within the application of preoperative cerebral hypoperfusion ***prediction***. We applied and presented simulations on a large cohort of patients with symptomatic carotid stenosis, for which this type of analysis is highly relevant with respect to preoperative planning of CEA. Relating our predictive approach to other perfusion monitoring parameters could in future prospective studies contribute with important knowledge regarding the link between perfusion pressure and the resulting intraoperative cerebral perfusion.

4.2. Importance of modeled mean arterial pressure

An important feature of our model is that it can be used to investigate the effect of a regulated blood pressure on the cerebral perfusion pressure. Since the cerebrovascular resistance was constant in our model, the flow rates in the geometry increased in the simulation with the 10-mmHg upregulated MAP, resulting in an increased pressure drop across the geometry. Due to these pressure drops, only 42% of the MAP increase was transferred to the stump pressure on the ipsilateral side. For the patients with support from the posterior circulation through the PCoAs, the stump pressure increase from the upregulation was 50%, reflecting the lower pressure drop with patent PCoAs. Knowledge of the magnitude of these expected responses could be important during surgery if one wishes to increase the stump pressure by raising MAP through medication.

For a clinical application, the intraoperative MAP will not be available in planning. We used MAP values measured during clamping in our analysis for stump pressure prediction, which gave a mean MAP of 101 mmHg. That was 8 mmHg higher than the average MAP assessed before surgery. The deviation in pressures supports that to best simulate the conditions during surgery, an expected MAP according to the surgical protocol (MAP = 100 mmHg) is recommended as input to the CFD model.

An alternative approach is to use these simulations to make a patient-specific estimate of the MAP required during clamping to receive a SP_{CFD} of, for example, 60 mmHg. An estimated lower MAP limit could then be used in the preoperative preparation since it simulates the required MAP needed during surgery. If the required MAP is considered critically high, it would indicate a need for shunting.

4.3. Difference in pressure between anatomical variations of the circle of Willis

The stump pressure has been suggested to result from the presence and size of ACoA or PCoA, degree of contralateral ICA stenosis, and mean arterial pressure (DePippo et al., 1999; Schneider et al., 1988; Wang et al., 2016). We found higher stump pressures in patients with a present ipsilateral PCoA than in those where it was absent. This pattern was found for patients with both uni- and bilateral stenoses. In all the patients with communication between the posterior and anterior circulation, sufficiently high stump pressures were found (range 50–78 mmHg) for our target limit of 50 mmHg. The single patient having a stump pressure < 60 mmHg had a relatively thin ipsilateral PCoA and a contralateral stenosis >75%. Information about present arteries can be deduced already from CTA, implying that a preoperative simulation using CFD may not be necessary for the subgroup with present PCoAs.

Our results suggest that if an ipsilateral PCoA is visible in CTA, in addition to present anterior segments, it may give sufficient collateral activation to avoid the need for shunting. This was in line with previous associations between an absent collateral support via PCoA and ACoA, and a higher frequency of shunt insertions (DePippo et al., 1999; Schneider et al., 1988; Schwartz et al., 1992; Wain et al., 1999). For patients with an absent PCoA, our stump pressures ranged between 40 and 60 mmHg, i.e., around the critical limit for shunt need, indicating that the CFD simulation may be useful in surgical planning. This was also supported by the significant decrease in modeled blood flow rate in the MCA. These findings should be interesting to investigate in a larger cohort.

4.4. Limitations of the CFD model

We proposed a model approach with patient-specific geometries and flow rates, which provided a good group-level agreement, although we still observed some individual variations. These discrepancies might have arisen from the imaging modalities, such as the time interval between the CTA and MRI investigation potentially affecting the segmented arterial sizes, or random variations in flow rates between repeated measurements. Discrepancies might also depend on model assumptions concerning autoregulatory effects, individual pressure drops along the carotid arteries, and the segmentation of high-degree stenoses. We consider the general agreement promising for predicting cerebral perfusion pressures, but possible limitations should be addressed in evaluations of larger cohorts.

Our assumption about the autoregulation was that the distal cerebrovascular resistances were constant. In practice, the autoregulatory system will likely reduce the resistance during clamping to increase the blood flow. Therefore, a CFD model with constant cerebrovascular resistance could potentially underestimate the flow rates and overestimate the stump pressure. However, vasopressors given during surgery for increasing blood pressure can have a cerebrovascular vasoconstrictive effect, possibly leaving the assumption of a constant cerebrovascular resistance a reasonable choice, supported by the group-level agreement between SP_{CFD} and SP_{Meas}.

The CTA was performed before surgery and not during clamping. Therefore, we were unaware of how (existing) PCoAs not visible on CTA responded to the clamping. However, if the PCoAs would inflate during clamping, the SP_{CFD} of those in the absent PCoA group should have been severely underestimated. That was not the case, supporting that the non-visible PCoAs did not inflate. Another limitation to this study was that it did not include any patients with an absent ACA1 or ACoA.

For the four cases with bilateral PCoAs, consistent flow boundary conditions in the first simulation could only be fulfilled using one PCoA. For these cases, we chose to keep the ipsilateral PCoA, because it was closer to the site of the stump pressure assessment. Since the consequence of omitting the contralateral PCoA should be limited to uncertainty in the contralateral PCA2 resistance, we believe the potential

effect on the estimated stump pressure is small compared to other uncertainties.

The outlier with an overestimated SP was suspected to be caused by a too widely segmented ACoA, causing a small pressure drop across the geometry. The outlier with an underestimated SP was potentially caused by a suspected low preoperative MAP, leading to a low vascular resistance and an overestimated pressure drop. In the latter case, this deviation highlights the importance of pressure monitoring during the MRI investigation, which was not available in this inclusion.

We had no reference stump pressures <40 mmHg. This might be an effect of the increased systolic blood pressure before clamping, but also an effect of only including patients with less severe symptoms, shown by the low mRS and NIHSS scores.

5. Conclusions

This study proposed and evaluated a CFD approach for predicting cerebral perfusion pressures during CEA. The analysis further revealed the influence of the ipsilateral PCoA and a potential contralateral carotid stenosis for CEA perfusion pressures. The agreement between the modeled and measured stump pressures indicated that our CFD approach could be useful in the preoperative planning of vascular interventions.

Funding

This work was supported by the Swedish Research Council [grant numbers 2015–05616 (AE), 2017–04949 (AW)]; the County Council of Västerbotten (AE, AW, JM); and the Swedish Heart Lung Foundation [grant number 20140592 (JM)].

CRediT authorship contribution statement

Madelene Holmgren: Conceptualization, Data curation, Formal analysis, Methodology, Project administration, Software, Visualization, Writing – original draft, Writing – review & editing. **Petter Holmlund:** Conceptualization, Formal analysis, Methodology, Software, Visualization, Writing – original draft, Writing – review & editing. **Karen-Helene Støverud:** Conceptualization, Methodology, Writing – review & editing. **Laleh Zarrinkoob:** Data curation, Investigation, Methodology, Resources, Writing – review & editing. **Anders Wåhlin:** Data curation, Funding acquisition, Methodology, Resources, Writing – review & editing. **Jan Malm:** Conceptualization, Data curation, Funding acquisition, Investigation, Methodology, Resources, Supervision, Writing – review & editing. **Anders Eklund:** Conceptualization, Data curation, Formal analysis, Funding acquisition, Investigation, Methodology, Project administration, Resources, Supervision, Writing – original draft, Writing – review & editing.

Declaration of Competing Interest

The authors declare that they have no known competing financial interests or personal relationships that could have appeared to influence the work reported in this paper.

Appendix A. Supplementary data

Supplementary data to this article can be found online at https://doi.org/10.1016/j.clinbiomech.2022.105827.

References

AbuRahma, A.F., Mousa, A.Y., Stone, P.A., Hass, S.M., Dean, L.S., Keiffer, T., 2011. Correlation of intraoperative collateral perfusion pressure during carotid endarterectomy and status of the contralateral carotid artery and collateral cerebral blood flow. Ann. Vasc. Surg. 25, 830–836.

Berg, P., Stucht, D., Janiga, G., Beuing, O., Speck, O., Thévenin, D., 2014. Cerebral blood flow in a healthy circle of Willis and two intracranial aneurysms: computational fluid dynamics versus four-dimensional phase-contrast magnetic resonance imaging. J. Biomech. Eng. 136, 1–9.

Cassot, F., Zagzoule, M., Marc-Vergnes, J.-P., 2000. Hemodynamic role of the circle of Willis in stenoses of internal carotid arteries. An analytical solution of a linear model. J. Biomech. 33, 395–405.

Cieslicki, K., Ciesla, D., 2005. Investigations of flow and pressure distributions in physical model of the circle of Willis. J. Biomech. 38, 2302–2310.

DePippo, P.S., Ascher, E., Scheinman, M., Yorkovich, W., Hingorani, A., 1999. The value and limitations of magnetic resonance angiography of the circle of Willis in patients undergoing carotid endarterectomy. Cardiovasc. Surg. 7, 27–32.

Domenick Sridharan, N., Thirumala, P., Chaer, R., Balzer, J., Long, B., Crammond, D., Makaroun, M., Avgerinos, E., 2018. Predictors of cross-clamp-induced intraoperative monitoring changes during carotid endarterectomy using both electroencephalography and somatosensory evoked potentials. J. Vasc. Surg. 67, 191–198.

Dunås, T., Holmgren, M., Wåhlin, A., Malm, J., Eklund, A., 2019. Accuracy of blood flow assessment in cerebral arteries with 4D flow MRI: evaluation with three segmentation methods. J. Magn. Reson. Imaging 50, 511–518.

Folstein, M.F., Folstein, S.E., McHugh, P.R., 1975. "Mini-mental state": a practical method for grading the cognitive state of patients for the clinician. J. Psychiatr. Res. 12, 189–198.

Gu, T., Korosec, F.R., Block, W.F., Fain, S.B., Turk, Q., Lum, D., Zhou, Y., Grist, T.M., Haughton, V., Mistretta, C.A., 2005. PC VIPR: a high-speed 3D phase-contrast method for flow quantification and high-resolution angiography. Am. J. Neuroradiol. 26, 743–749.

Hans, S.S., Jareunpoon, O., 2007. Prospective evaluation of electroencephalography, carotid artery stump pressure, and neurologic changes during 314 consecutive carotid endarterectomies performed in awake patients. J. Vasc. Surg. 45, 511–515.

Holmgren, M., Wåhlin, A., Dunås, T., Malm, J., Eklund, A., 2020. Assessment of cerebral blood flow pulsatility and cerebral arterial compliance with 4D flow MRI. J. Magn. Reson. Imaging 51, 1516–1525.

Holmgren, M., Støverud, K.-H., Zarrinkoob, L., Wåhlin, A., Malm, J., Eklund, A., 2021. Middle cerebral artery pressure laterality in patients with symptomatic ICA stenosis. PLoS One e0245337, 1–15.

Howell, S.J., 2007. Carotid endarterectomy. Br. J. Anaesth. 99, 119–131.

Johnson, K.M., Markl, M., 2010. Improved SNR in phase contrast velocimetry with five-point balanced flow encoding. Magn. Reson. Med. 63, 349–355.

Jonsson, M., Lindström, D., Wanhainen, A., Djavani Gidlund, K., Gillgren, P., 2017. Near infrared spectroscopy as a predictor for shunt requirement during carotid endarterectomy. Eur. J. Vasc. Endovasc. Surg. 53, 783–791.

Liu, J., Yan, Z., Pu, Y., Shiu, W.-S., Wu, J., Chen, R., Leng, X., Qin, H., Liu, X., Jia, B., Song, L., Wang, Yilong, Miao, Z., Wang, Yongjun, Liu, L., Cai, X., 2017. Functional assessment of cerebral artery stenosis: a pilot study based on computational fluid dynamics. J. Cereb. Blood Flow Metab. 37, 2567–2576.

Malm, J., Jacobsson, J., Birgander, R., Eklund, A., 2011. Reference values for CSF outflow resistance and intracranial pressure in healthy elderly. Neurology 76, 903–909.

Marshall, I., Papathanasopoulou, P., Wartolowska, K., 2004. Carotid flow rates and flow division at the bifurcation in healthy volunteers. Physiol. Meas. 25, 691–697.

Matsuura, S., Takayama, T., Yuhn, C., Oshima, M., Shirasu, T., Akai, T., Isaji, T., Hoshina, K., 2021. Carotid stump pressure and contralateral internal carotid stenosis ratio during carotid endarterectomies: 1D-0D hemodynamic simulation of cerebral perfusion. Ann. Vasc. Dis. 14, 39–45.

Merkkola, P., Tulla, H., Ronkainen, A., Soppi, V., Oksala, A., Koivisto, T., Hippeläinen, M., 2006. Incomplete circle of Willis and Right axillary artery perfusion. Ann. Thorac. Surg. 82, 74–79.

Moritz, S., Kasprzak, P., Arlt, M., Taeger, K., Metz, C., 2007. Accuracy of cerebral monitoring in detecting cerebral ischemia during carotid endarterectomy. Anesthesiology 107, 563–569.

Müller, M.D., Seidel, K., Peschi, G., Piechowiak, E., Mosimann, P.J., Schucht, P., Raabe, A., Bervini, D., 2021. Arterial collateral anatomy predicts the risk for intraoperative changes in somatosensory evoked potentials in patients undergoing carotid endarterectomy: a prospective cohort study. Acta Neurochir. 163, 1799–1805.

Naylor, A., Ricco, J.-B., de Borst, G., Debus, S., de Haro, J., Halliday, A., Hamilton, G., Kakisis, J., Kakkos, S., Lepidi, S., Markus, H., McCabe, D., Roy, J., Sillesen, H., van den Berg, J., Vermassen, F., 2018. Editor's choice - management of atherosclerotic carotid and vertebral disease: 2017 cinical practice guidelines of the european society for vascular surgery (ESVS). Eur. J. Vasc. Endovasc. Surg. 55, 142.

North American Symptomatic Carotid Endarterectomy Trial, 1991. Methods, patient characteristics, and progress. Stroke 22, 711–720.

Pennekamp, C.W.A., Van Laar, P.J., Hendrikse, J., Den Ruijter, H.M., Bots, M.L., Van Der Worp, H.B., Kappelle, L.J., Buhre, W.F., Bleys, R.L.A.W., Moll, F.L., De Borst, G.J., 2013. Incompleteness of the circle of Willis is related to EEG-based shunting during carotid endarterectomy. Eur. J. Vasc. Endovasc. Surg. 46, 631–637.

Schneider, P.A., Bernd Ringelstein, E., Rossman, M.E., Dilley, R.B., Sobel, D.F., Otis, S.M., Bernstein, E.F., 1988. Importance of cerebral collateral pathways during carotid endarterectomy. Stroke 19, 1328–1334.

Schollenberger, J., Osborne, N.H., Hernandez-Garcia, L., Figueroa, C.A., 2021. A combined computational fluid dynamics and arterial spin labeling MRI modeling strategy to quantify patient-specific cerebral hemodynamics in cerebrovascular occlusive disease. Front. Bioeng. Biotechnol. 9, 1–15.

Schwartz, R.B., Jones, K.M., LeClercq, G.T., Ahn, S.S., Chabot, R., Whittemore, A., Mannick, J.A., Donaldson, M.C., Gugino, L.D., 1992. The value of cerebral

angiography in predicting cerebral ischemia during carotid endarterectomy. AJR 159, 1057–1061.
van Sweiten, J.C., Koudstaal, P.J., Visser, M.C., Schrouten, H.J.A., van Gijn, J., 1988. Interobserver agreement for the assessment of handicap in stroke patients. Stroke 19, 604–607.
Wåhlin, A., Eklund, A., Malm, J., 2021. 4D flow MRI hemodynamic biomarkers for cerebrovascular diseases. J. Intern. Med. 1–13.
Wain, R.A., Veith, F.J., Berkowitz, B.A., Legatt, A.D., Schwartz, M., Lipsitz, E.C., Haut, S. R., Bello, J.A., 1999. Angiographic criteria reliably predict when carotid endarterectomy can be safely performed without a shunt. J. Am. Coll. Surg. 189, 93–100.
Wang, B.H., Leung, A., Lownie, S.P., 2016. Circle of Willis collateral during temporary internal carotid artery occlusion II: observations from computed tomography angiography. Can. J. Neurol. Sci. 43, 538–542.
Wiske, C., Arhuidese, I., Malas, M., Patterson, R., 2018. Comparing the efficacy of shunting approaches and cerebral monitoring during carotid endarterectomy using a national database. J. Vasc. Surg. 68, 416–425.
Zarrinkoob, L., Ambarki, K., Wåhlin, A., Birgander, R., Eklund, A., Malm, J., 2015. Blood flow distribution in cerebral arteries. J. Cereb. Blood Flow Metab. 35, 648–654.
Zarrinkoob, L., Wåhlin, A., Ambarki, K., Birgander, R., Eklund, A., Malm, J., 2019. Blood flow lateralization and collateral compensatory mechanisms in patients with carotid artery stenosis. Stroke 50, 1081–1088.